Real-time Simulations and Experiments on Surface Acoustic Wave Scattering in Periodic Microstructures

István A. Veres,[1,*] Dieter M. Profunser,[2]
Oliver B. Wright,[2] Osamu Matsuda,[2] and Brian Culshaw[1]

[1]*Department of Electronic and Electrical Engineering, Centre for Ultrasonic Engineering, University of Strathclyde, Glasgow G1 1XW, United Kingdom*
[2]*Department of Applied Physics, Graduate School of Engineering, Hokkaido University, Sapporo, 060-8628, Japan*

(Received April 8, 2010)

Surface acoustic wave scattering in periodically microstructured surfaces is investigated numerically and experimentally. We perform the simulations by a real-time finite element technique and experiments by ultrashort pulsed optical excitation and interferometric detection. Good agreement is obtained between simulation and experiment. Our results clearly show the opening of phononic stop bands of the excited Rayleigh-like waves at the Brillouin zone boundary. In addition, we investigate the influence of the grating thickness by numerical simulations. Our results show the strong influence of the grating thickness on the position and width of the phononic stop bands.

PACS numbers: 63.20.D-, 62.65.+k, 68.35.Iv

I. INTRODUCTION

Acoustic wave propagation in samples with spatial periodicity can be used to study their phononic band structure. Such phononic crystals (PCs) possess stop bands where the acoustic waves are significantly damped. Longitudinal and shear acoustic waves can be used for the characterization of phononic crystals in the form of bulk microstructures or nanostructures [1–4]. Surface acoustic waves (SAWs) have been used to investigate microstructured phononic crystals [5]. Several experimental techniques can be used to study such samples, such as the use of low-temperature phonon imaging or Brillouin scattering [6–8], but it has been shown to be particularly effective to use laser-pulse generation and spatiotemporal imaging of SAWs [9, 10]. Single-point excitation and imaging of a surface by the latter method allows the acoustic dispersion relation for surface waves to be extracted, including the directional band structure, by simply taking Fourier transforms [11].

Examples of surface phononic crystals that have been imaged are one-dimensional phononic crystals (1DPCs), such as periodically alternating lines with different acoustic properties [11], or two-dimensional phononic crystals (2DPCs), such as periodic 2D lattices of cylindrical holes [12]. Such surface phononic crystals are important in filtering applications up to gigahertz frequencies [13, 14].

Time-domain finite element (FEM) or finite difference methods (FDTD) are commonly used for the real-time simulation of wave propagation phenomena, including acoustic

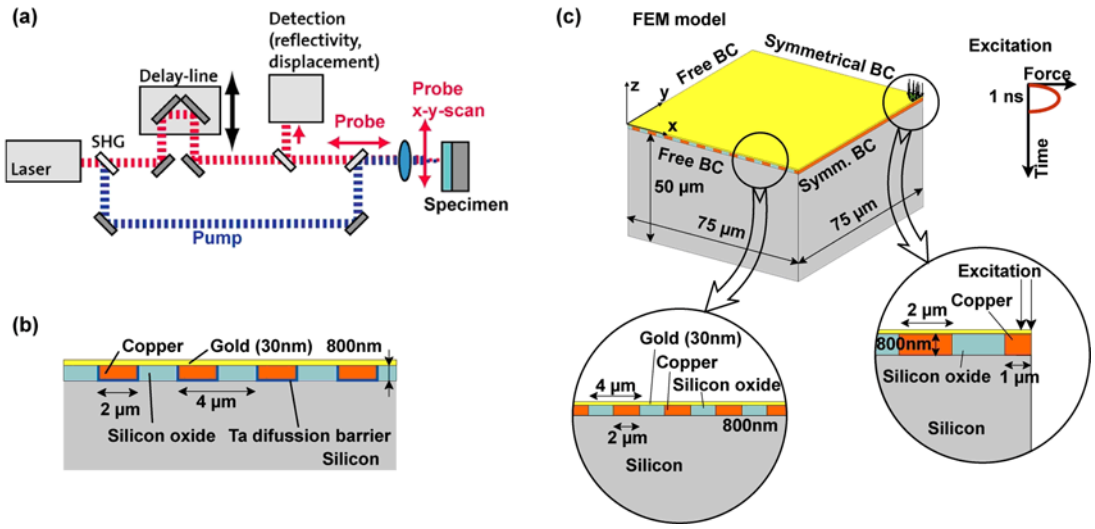

FIG. 1: (a) Experimental setup. (b) 1DPC sample for the experiment. The phononic crystal is formed from alternating copper and silicon oxide lines. (c) FEM model of a 1DPC with the applied excitation. The gold layer has a thickness of 30 nm and the copper and silicon oxide lines are 800-nm thick and 2-μm wide, respectively, for the first structure studied. BC: boundary condition.

propagation [15–17]. These applications are sometimes carried out on quasi-2D structures such as plates or discs, in which case their thickness can be modeled with a few elements. For thicker samples, as in the present study, the modeling of SAWs and particularly their scattering in a periodic structure requires larger 3D models wherein the number of the nodes can be on the order of 10^8 or higher.

Here, we investigate experimentally and numerically the interaction of laser-generated SAWs with 1D micro-fabricated phononic crystals that possess stop bands at ultrahigh frequencies (0.2–1 GHz). The complex structure of the stop bands and the hybridization of the different wave modes in similar 1D geometries was predicted theoretically and investigated experimentally several times [7, 11, 18–20]. The simulations presented here allow the analysis of the acoustic wave scattering in the time and frequency domains and can be directly compared with the experimental results. By studying the influence of a geometrical parameter - the grating thickness - on the scattered wave field in the numerical simulations, we demonstrate one way of optimizing the acoustic features of this phononic crystal.

We first briefly describe the measurement and the simulation techniques and compare the experimental results with the simulations. We then describe the influence of the grating thickness on the acoustic stop bands by means of simulations.

II. EXPERIMENT AND REAL-TIME SIMULATION

A. Experimental setup and sample

The pump light pulses of duration ∼200 fs and wavelength of 400 nm are absorbed at a ∼2-μm-diameter spot on the surface of the sample. The thermoelastically-excited stress field launches SAWs with displacements in the 10 pm range. The broadband SAW pulses contain frequencies up to ∼1.3 GHz with the maximum amplitude between 200 MHz and 700 MHz [12]. A common-path Sagnac interferometer [Fig. 1(a)] is used to measure the induced optical phase difference $\Delta\phi$ between probe optical pulses in two beams that are focused with a delay time difference of 300 ps to a similar spot size [9, 12, 21]. The out-of-plane velocity of particle motion induced by the surface acoustic waves is thus imaged across the sample surface by scanning the probe spot (over an area of 100×100 μm^2). Typically, 40 images over a time period of 13.1 ns, corresponding to a 76.3 MHz repetition rate, are recorded.

The 1DPC is formed from alternating polycrystalline copper and silicon oxide lines deposited perpendicular to the [011] direction on a (100) silicon substrate [see Fig. 1 (b)]. The lines are 2 μm wide (period $a = 4$ μm) and have a thickness of 800 nm in the experiment. For the simulations, we considered various thicknesses. A 25-nm tantalum layer serves as a diffusion barrier for the copper, and a 30-nm polycrystalline gold layer is sputtered at the top of the specimen to achieve uniform reflectivity [Fig. 1(b)].

B. Real-time simulation

The propagation of the SAWs is modeled using the FEM package PzFlex (FlexLab, Weidlinger A. Inc.) with 3D elements (each with eight nodes) arranged on an orthogonal grid. To reduce the effect of the reflections at the edges and to obtain a better wave number (k_x, k_y) resolution, a 150×150 μm^2 area of the sample was modeled. We make use of the crystal and geometrical symmetry of the 1DPC in the simulations by the incorporation of appropriate symmetrical boundary conditions [see Fig. 1(c)]. The model includes the thin gold layer, which has significantly different acoustic impedances and sound velocities compared to copper or silica. Tantalum is, however, acoustically similar to copper, and so we neglect this layer [Fig. 1(c)].

The spatial discretisation of the model consists of elements with average dimensions of $0.095 \times 0.095 \times 0.10$ μm^3 ($dx \times dy \times dz$) at the top. The gold layer is represented by one element over its thickness. The height of the elements in the silicon is progressively increased to $dz = 0.38$ μm at the bottom of the sample in order to reduce the time of the computation. The model consists of approximately 10^8 nodes and requires 5370 time steps corresponding to 39.3 ns.

The properties of the materials used are given in Table I: copper, silica, and gold were modeled as isotropic materials; silicon was taken to be cubic. In our simulations the temporal discretisation is in the range of 5–10 ps, which is calculated by software on

TABLE I: Material properties for copper, gold, tantalum, silicon oxide, and silicon.

	ρ [kg/m^3]	c_{11} [GPa]	c_{12} [GPa]	c_{44} [GPa]
Cu[a]	8930	201.71	05.98	47.86
Au[a]	19300	207.53	151.3	28.12
SiO[a]	2200	71.20	22.79	24.21
Si[b]	2330	194.55	63.9	79.6

[a]Cu, Au, and SiO are assumed to be isotropic.
[b]The cubic symmetry of crystalline Si is taken into account.

the basis of the criteria for numerical stability. The calculated surface displacements were saved for every 15th time step (i.e., at an interval of approximately 100 ps). The total duration of the simulation was 39.3 ns, which is three-times longer than the duration of the experimental data, resulting in better frequency resolution for the simulation. This is possible by the use of a larger surface area; the relatively slow point-excited SAWs require 25 ns to occupy the whole simulated surface. The laser generation of the surface waves is modeled by a short vertical impulsive force of 1 ns duration (in the form of half a period of a sine function) applied over a uniform circular region of radius 1 μm [Fig. 1(c)]. These conditions are chosen to give approximate agreement with the experimentally observed frequency spectrum of the SAWs. According to the four-fold symmetry of the model, only one quarter of the sample area needs to be included in the simulation.

III. RESULTS AND DISCUSSION

A. Comparison of simulated and experimental dispersion relations

The complete dispersion relation of the SAWs can be evaluated from the real-time images using a combination of Fourier transforms: 2D in the spatial domain and 1D in the temporal domain [12]:

$$F(\mathbf{k},\omega) = \frac{1}{(2\pi)^3} \int_{-\infty}^{\infty} \int_{-\infty}^{\infty} f(\mathbf{r},t) e^{i(\omega t - \mathbf{k}\cdot\mathbf{r})} d^2\mathbf{r} dt \tag{1}$$

where $f(\mathbf{r}, t)$ is the acoustic disturbance, $\mathbf{r}$ is the position vector, $\mathbf{k}$ is the 2D wave vector, and ω is the angular frequency. The resulting function $F(\mathbf{k},\omega)$ is related to the dispersion relation of the SAWs since this Fourier transform is nonzero only for $\mathbf{k}$-ω pairs which satisfy the dispersion relation. We first compare the experimental and the simulation results. We then study the influence of the grating thickness on the dispersion relation and the stop bands.

Real-time images for the numerical simulation for $f(\mathbf{r}, t)$ are shown in the next subsection. Those for the experiment are given elsewhere, and are not reproduced here

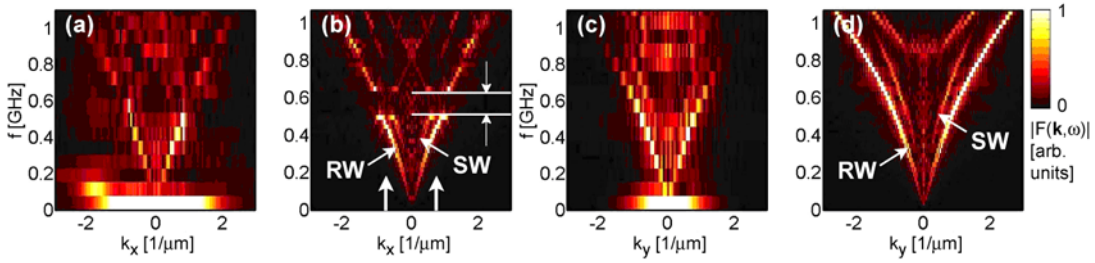

FIG. 2: Cross sections of the experimental, (a) and (c), and the simulated, (b) and (d) spatiotemporal Fourier transforms $|F|$ in the direction (x) perpendicular to the lines, (a)–(b) and in the direction (y) along the lines (c)–(d). The period of the grating is a= 4 μm with a thickness of h= 0.8 μm. The upwardly directed arrows in (b) show the edges of the 1st Brillouin zone.

[11]. Experiment and simulation are best compared in the frequency domain shown in Fig. 2, we show the cross sections of the Fourier transform $|F|$ as a frequency-wavenumber plot for the x and y directions, obtaining good agreement between the experimental and numerical dispersion relations, where the x direction is taken perpendicular to the lines. For the experimental analysis, f corresponds to the outward surface velocity, whereas in the simulation, f corresponds to the outward surface displacement. An extra factor of $i\omega$ was applied to the temporal Fourier transform in the simulation to account for this difference. For the present case of an acoustically slow grating layer on a fast substrate, two acoustic branches are predicted [19, 24]: Rayleigh-like waves (RW) and higher-phase-velocity Sezawa-waves (SW). These modes can be seen below 500 MHz in the x direction in the simulation (but not so clearly in experiment) and up to 1 GHz in the y direction. They have also been detected previously in similar samples [19, 22, 23]. The dispersion curves are bent because of the finite layer thickness; on increasing the acoustic frequency, the SAW penetration depth decreases, resulting in a higher proportion of the surface motion shifting into the grating and thus producing dispersion. The x-directed waves [see Fig. 2(a)–(b)] exhibit a stop band between 500 and 600 MHz close to the boundary of the first Brillouin zone (1st BZ) at $k_x = \pm\, \pi/a = \pm\, 0.79\ \mu\text{m}^{-1}$, where a is the grating period, similar to the behavior observed elsewhere for similar samples [12, 18, 19].

B. Effect of the grating thickness

In engineering applications, such as in SAW filtering, the location and the size of the stop band is crucial. For model-based design and optimization, several geometrical and material parameters such as grating period a, grating thickness h, and the strength of the periodicity (depending on the acoustic properties of the lines) can be varied. Here we choose the example of varying the grating thickness to obtain different values for a/h and evaluate its influence on the position and width of the phononic stop band.

The results of the simulation are shown in the frequency and temporal domains in Fig. 3 for three different grating thicknesses h with a= 4 μm. Stop bands are observed

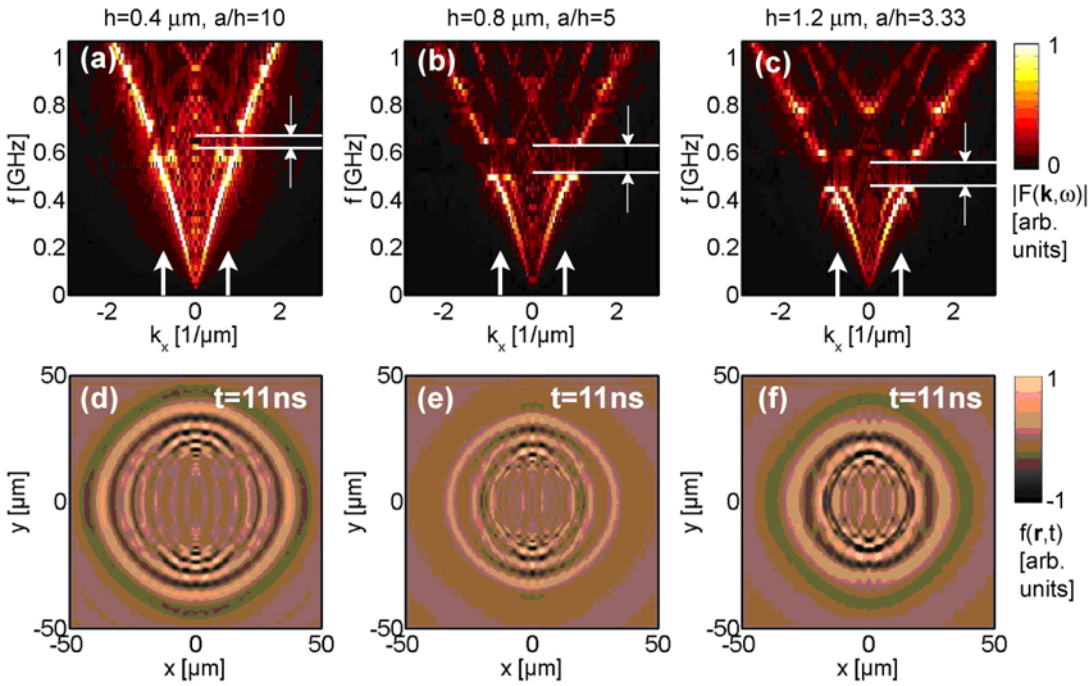

FIG. 3: (a)–(c) ω-k_x cross sections of the numerical dispersion relations in the x direction obtained from the spatiotemporal Fourier transforms $|F(\mathbf{k},\omega)|$ for gratings of period $a = 4.0$ μm and thicknesses h= 0.4, 0.8, and 1.2 μm, respectively. The position and the extent of the stop band shows a strong dependence on h. (d)–(f) Time domain images of the simulated surface displacement for different respective grating thicknesses, corresponding to a time t= 11 ns after excitation. The different extents of the wave fronts are a consequence of different dispersion relations.

close to the 1st BZ boundary (see arrows) as before. For the thinnest grating with h= 0.4 μm, the dispersion is negligible for frequencies below ∼0.5 GHz (i.e., the dispersion curve is straight), giving sound velocities of ∼4500 and ∼7200 m s^{-1} for the RW and SW branches, respectively. Two maxima near the BZ boundaries at the bottom of the stop band are the result of an avoided crossing between RW and SW branches [19]. For the thicker gratings with h ranging from 0.8 to 1.2 μm, the curvature of the dispersion curve becomes progressively stronger with thickness, causing the frequency of the stop band to decrease. Due to this effect, a further stop band becomes visible at ∼800 MHz (h= 0.8 μm) and at ∼700 MHz (h= 1.2 μm). We interpret this as being the result of an avoided crossing between RW branches. The width of the first stop band is larger for h= 0.8 μm than for h= 0.4 μm, as might be expected from the increased scattering potential, but, perhaps surprisingly, the stop band for h= 1.2 μm is reduced in width compared to that for h= 0.8 μm. The stronger curvature of the dispersion curve for h= 1.2 μm may be responsible for this. The strength of the SW modes also varies with the grating thickness and decreases with decreasing h. These findings should be easier to understand by performing additional simulations for intermediate values of h.

The different extent of wave travel in the time domain images [Fig. 3 (d)–(f)] reflects the different dispersion relations. For h= 1.2 μm, the waves are slower than those for h= 0.4 μm; in the former case, the velocity is closer to the Rayleigh velocity of an effective medium comprised of polycrystalline copper and silicon oxide, whereas in the latter case, the velocity is closer to the Rayleigh-wave velocity in silicon (100) in the [011] direction ($\sim$4800 m s^{-1}).

IV. CONCLUSIONS

In conclusion, we have studied the propagation characteristics of surface acoustic waves in 1DPCs by a real-time imaging method and by numerical (FEM) analysis. The dispersion relations were obtained by spatiotemporal Fourier transforms. We found good agreement between the results of the simulations and those of the experiments, particularly with regard to the width and position of the phononic stop band.

Further simulations reveal the effects of the grating thickness on the phononic band structure. Our results demonstrate a complex dependence of the band structure on the grating thickness, with the largest stop band being found for a grating thickness of $\sim$0.8 μm (a/h= 5). These numerical and experimental methods are appropriate for studying other wave propagation phenomena such as surface acoustic wave resonators, waveguides, and 2D or 3D phononic crystals.

Acknowledgments

Two of the authors, IAV and BC acknowledge the support of the UK EPSRC.

References

* Electronic address: istvan.veres@eee.strath.ac.uk

[1] M. S. Kushwaha, Int. J. Mod. Phys. B **977** (1996)
[2] M. Sigalas *et al.*, Z. Kristallogr. **220** 765 (2005).
[3] F. S. Hickernell, in Physical Acoustics, Vol. 24, edited by R. N. Thurston, A. D. Pierce, and E. P. Papadakis (Academic, London, 1999), p. 135.
[4] V. Narayanamurti *et al.*, Phys. Rev. Lett. **43**, 2012 (1979).
[5] T. T. Wu, L. C. Wu and Z. G. Huang, J. Appl. Phys. **97**, 094916 (2005).
[6] D. C. Hurley, S. Tamura, J.P. Wolfe and H. Morkoc, Phys. Rev. Lett **58**, 2446 (1987).
[7] J. R. Dutcher *et al.*, Phys. Rev. Lett. **68**, 2464 (1992).
[8] J . T. Gorishnyy et al., Phys. Rev. Lett. **94**, 115501 (2005).
[9] Y. Sugawara *et al.*, Appl. Phys. Lett. **83**, 1340 (2003).
[10] T. Tachizaki, *et al.*, Rev. Sci. Instr., **77**, 043713 (2006).
[11] D. M. Profunser, O. B. Wright and O. Matsuda, Phys. Rev. Lett. **97**, 055502 (2006).
[12] D. M. Profunser, E. Muramoto, O. Matsuda and O. B. Wright, Phys. Rev. B **80**, 014301 (2009).
[13] S. Mohammadi, A. A. Eftekhar, W. D. Hunt, and A. Adibi, Appl. Phys. Lett. **94**, 051906

(2009).
[14] S. Benchabane, A. Khelif, J. Y. Rauch, L. Robert and V. Laude, Phys. Rev. E **73**, 065601 (2006).
[15] K.-J. Bathe, *Finite Element Procedures* (Prentice-Hall Inc, New Jersey, 1996).
[16] C. Giannetti, F. Banfi, D. Nardi, G. Ferrini and F. Parmigiani, IEEE Photonics J. **1**, 21, (2009)
[17] D. Gsell, T. Leutenegger, and J. Dual, J. Acoust. Soc. Am. **116**, 3284 (2004).
[18] L. Giovannin and F. Nizzoli, Phys. Rev. Lett. **69**, 1572 (1992).
[19] A. A. Maznev, Phys. Rev. B **78**, 155323 (2008).
[20] M. M. de Lima, Phys. Rev. Lett. **104**, 165502 (2010).
[21] Y. Sugawara, *et al.*, Phys. Rev. Lett. **88**, 185504 (2002).
[22] A. A. Maznev and A. G. Every, J. Appl. Phys. **106**, 113531 (2009).
[23] A. A. Maznev and O. B. Wright, J. Appl. Phys. **105**, 123530 (2009).
[24] B. A. Auld, *Acoustic Fields and Waves in Solids*, 2th ed. (Krieger Publishing Company, Malabar, 1990).